Electronic Supporting Information

Evaluation of the catalytic activity of metal phosphates and related oxides in the ketonization of propionic acid

Jacopo De Maron [1,*], Luca Bellotti [1], Alessio Baldelli [1], Andrea Fasolini [1], Nicola Schiaroli [2], Carlo Lucarelli [2], Fabrizio Cavani [1], and Tommaso Tabanelli [1,*]

1 Dipartimento di Chimica Industriale "Toso Montanari", Alma Mater Studiorum Università di Bologna, Viale Risorgimento 4, 40136 Bologna, Italy.
2 Dipartimento di Scienza e Alta Tecnologia, Università degli Studi dell'Insubria, Via Valleggio 11, 22100, Como, Italy.
* Correspondence: tommaso.tabanelli@unibo.it; jacopo.demaron2@unibo.it

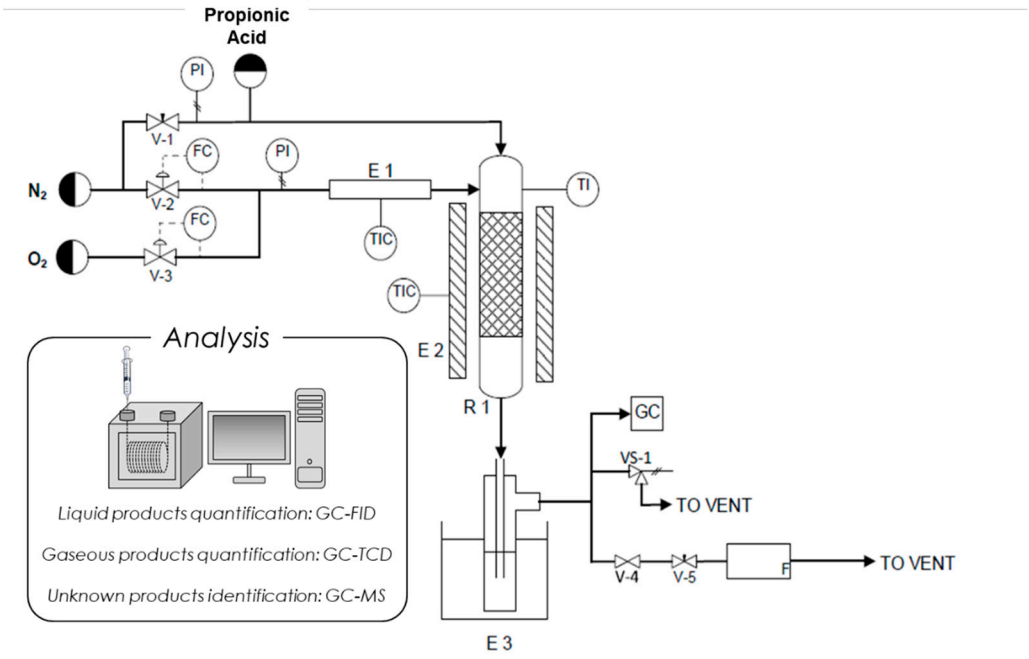

Figure S1. Schematic illustration of the gas-phase plant and the analytical system used to carry out the catalytic tests. Symbols: PI = pressure indicator, FC = mass flow controller, TIC-E1 = temperature controller and heating device (for carrier gas), TI = temperature indicator (catalytic bed), TIC-E2 = temperature controller and furnace, R1 = reactor, E3 = ice bath (to cool down the liquid product sampler), F = bubble flow meter.

Chapter S1: Detailed characterisation of the catalytic materials

S.1.1. Crystal structures and Phosphorus/Metal atomic ratios

Powder X-ray diffraction analyses were carried out to determine catalysts crystal structure and phase-purity. Commercial SiO_2 possesses the highest SSA (544 m^2/g) among the materials investigated, is amorphous, and its XRD powder pattern, shown in Figure S2a, is characterized by only one broad peak, centred at $2\theta = 23°$ and 20 degrees wide. Commercial Al_2O_3 (Figure S3a) shows the presence of a pure cubic γ-phase; this material is poorly crystalline due to the intrinsic defectivity of its spinel structure and possess a relatively high SSA of 159 m^2/g.

La_2O_3 (Figure S4a) consists of a pure hexagonal phase, is highly crystalline, and possess a relatively low SSA of 26 m^2/g due to the high calcination temperature of 750 °C required to de-compose the lanthanum carbonate precursor.

t-ZrO_2-PR possesses the highest value of SSA among the zirconium oxides investigated (123 m^2/g) and its diffractogram is characterized by the typical reflections of the tetragonal polymorph (Figure S5a); however, a shoulder at $2\theta = 28°$ suggests the presence of a small impurity of the monoclinic phase. Similarly, *m*-ZrO_2-PR diffractogram shows typical pattern of the monoclinic phase (Figure S6a), plus a very weak peak centred around $2\theta = 30°$, which is attributable to the

strongest reflection of a small impurity of the tetragonal polymorph. The diffraction pattern of *m*-ZrO_2-HT (Figure S7a) is less defined in respect to that of *m*-ZrO_2-PR, suggesting a lower degree of crystallinity and a higher defectivity, in agreement with its higher SSA (117 m^2/g instead of 36 m^2/g). Moreover, no reflection attributable to an impurity of the tetragonal phase are present; therefore, the hydrothermal synthesis with urea allows to obtain a monoclinic ZrO_2 with a much higher SSA and more phase-pure in respect to the conventional precipitation technique with NH_3.

Among the metal phosphates, La/P/O is the only one displaying a relatively well-defined diffraction pattern. Its diffractogram is characterized by broad reflections, attributable to a monoclinic $LaPO_4$ (monazite) phase (Figure S8a). However, the experimental P/La atomic ratio of 0.89 calculated from XRF spectra for this catalyst indicates that it is not stoichiometric and may explain its low crystallinity.

Al/P/O (Figure S9a), in agreement with the literature [1], is amorphous and its diffractogram is very similar to the one of SiO_2 because these two materials possess analogous structures. In this case the experimental P/Al atomic ratio (0.99) is in good agreement with the stoichiometry of $AlPO_4$ and no reflection attributable to the segregation of Al_2O_3 were found.

Zr/P/O is amorphous too; its diffraction pattern (Figure S10a) is characterized by a broad diffraction peak at around $2\theta = 20°$ and matches very well those reported previously by some authors [2, 3]. The experimental P/Zr atomic ratio = 1.46 for this sample matches quite well the one measured by Sushkevich et al [1] and is intermediate between the value of 1.34 expected from $Zr_3(PO_4)_4$ and the value of 2 expected from ZrP_2O_7 and the layered hydrogen phosphate phases α-$Zr(HPO_4)_2$*H_2O and γ-$Zr(H_2PO_4)(PO_4)$*$2H_2O$. This fact suggests that Zr/P/O is probably a mixture of different polymorphs, and that P is likely to be present not only as PO_4^{3-}, but also as HPO_4^{2-}, as $H_2PO_4^-$ and perhaps as $P_2O_7^{4-}$.

S.1.1. Surface acid/base properties

The densities of acidic sites and basic sites reported in Table 1 were measured by means of NH_3 and CO_2-TPD respectively and are expressed as $\mu mol/m^2$ to allow an easy comparison of the intrinsic acidity and basicity of materials with very different SSA.

Despite its very high SSA of 544 m^2/g, the TPD characterization (Figure S2b) indicates that commercial SiO_2 does not interact strongly with neither CO_2 nor NH_3. The mild acidity displayed by this materials (the desorbed NH_3 was 0.2 $\mu mol/m^2$, in good agreement with previous literature [4] is of the Brønsted type and arises from the presence of pending silanol groups (Si-OH) [5].

Al_2O_3 is a well-known amphoteric oxide possessing strong acidity (mainly of the Lewis type [6]) and weak basicity [7]. The TPD characterization confirmed that the commercial Al_2O_3 sample possesses a low density of basic sites (0.7 $\mu mol/m^2$) and a much larger density of acidic sites (5.2 $\mu mol/m^2$): these values are in good agreement with those reported previously by other authors [8, 9]. The NH_3-TPD profile (Figure S3b) for this material displays a broad desorption band that extends from 150 to 600 °C; the maximum of desorption is centred at 270 °C, with a significant shoulder around 215 °C. However, NH_3 desorbs in small amounts up to 600 °C therefore the material possesses a small fraction of strong acidic sites even though weak and medium-strength sites are predominant.

La_2O_3 is expected to be the most basic oxide among those investigated because lanthanides possess an intermediate basicity between alkali-earth metals and transition metals. Moreover, the very high calcination temperature of 750 °C required to decompose the lanthanum carbonates [10] formed during the synthesis due to the absorption of atmospheric CO_2 in the basic solution of the lanthanum hydroxide precursor is a clear indication of its basicity. The TPD characterization (Figure S4b) substantially confirmed these indications: the density of basic sites (6.7 $\mu mol/m^2$) is roughly ten times larger than the one of Al_2O_3 and the CO_2-TPD profile shows two maxima centred at 115 °C (weak basic sites) and at 485 °C (strong basic sites), the latter being largely pre-vailing. On the other hand, the amount of desorbed NH_3 was negligible, indicating that La_2O_3 do not possesses significant acidity. The results of both CO_2-TPD [11, 12] and NH_3-TPD [13] for La_2O_3 are in good agreement with the literature.

The TPD characterization of *t*-ZrO_2-PR, *m*-ZrO_2-PR and *m*-ZrO_2-HT is shown in Figure S5b, S6b and S7b respectively. The density of basic sites for these materials follows the order *m*-ZrO_2-HT (5.0 $\mu mol/m^2$) > *m*-ZrO_2-PR (3.5 $\mu mol/m^2$) > *t*-ZrO_2-PR (1.2 $\mu mol/m^2$), indicating that the CO_2 adsorption capacity of the monoclinic phase is higher than the one of tetragonal phase, in agreement with Pokrovski et al [14]. The CO_2-TPD profiles of all these three materials display a single desorption maximum centred between 120 and 140 °C and related to the presence of weak basic sites. However, the samples with the monoclinic crystal habit desorbed a significant amount of CO_2 up to 450 °C, while t-ZrO_2-PR did not; this is a clear indication that the monoclinic phase possesses not only a larger number but also stronger basic sites in respect to the tetragonal phase, in line with the results reported by Bachiller-Baeza et al [15]. The densities of acidic sites of *m*-ZrO_2-PR, *m*-ZrO_2-HT, and t-ZrO_2-PR instead are quite similar between each other (4.7, 4.3 and 4.1 $\mu mol/m^2$ respectively) and the NH_3-TPD profile of all three materials is characterized by a broad desorption peak that extends from 150

to 450 °C and is centred between 270 and 290 °C, indicating that weak, medium-strength and strong acidic sites are present on the surface of all three materials. The results of TPD characterization for *m*-ZrO_2-PR and *t*-ZrO_2-PR are in remarkably good agreement with those reported by Ding et al [16] and Blair Vasquez et al [17] respectively. On the other hand, the basic and acid density measured for *m*-ZrO_2-HT are 2-3 times higher than those reported by Ding et al for the same material [18]. Despite that, it is reasonable that the *m*-ZrO_2-HT catalyst, being more defective than *m*-ZrO_2-PR (as suggested by its lower crystallinity and its much higher SSA determined by means of XRD and BET characterizations) possesses a larger fraction of coordinatively unsaturated O^{2-} anions and basic hydroxyl groups, and therefore a stronger basicity. DRIFTS spectra were collected after adsorption of pyridine over m-ZrO_2-HT and desorption at increasing temperature in order to characterize the type of acidity (e.g. Lewis or Brønsted) displayed by monoclinic zirconia. These results are shown in Figure S11. The spectrum is characterized by the presence of three strong bands centred at 1603 cm^{-1}, 1575 cm^{-1} and 1443 cm^{-1} that are attributable to the presence of pyridine bonded to Lewis acidic sites [19]. The bands attributable to pyridine bonded to Brønsted acidic sites instead are absent (1637 cm^{-1}) or extremely weak (1558 cm^{-1}). The DRIFTS spectra recorded for tetragonal ZrO_2 by Blair Vasquez et al [17] are very similar to those reported in Figure S11 for monoclinic zirconia; therefore, it can be concluded that the acidity of both monoclinic and tetragonal zirconia is mainly of the Lewis type and their Brønsted acidity is very weak.

The TPD characterizations of La/P/O, Al/P/O and Zr/P/O are reported in Figure S8b, S9b and S10b respectively. The CO_2-TPD profiles of all three metal phosphates consist of a flat line, therefore it can be concluded that their basicity is so weak that does not lead to the adsorption of a detectable amount of CO_2, as it was for SiO_2. On the other hand, the density of acidic sites of these material (19.3, 13.0 and 10.4 µmol/m^2 for Al/P/O, Zr/P/O and La/P/O respectively) is 2 order of magnitude larger than the one of SiO_2 and ≥ 2-fold the one of Al_2O_3. It seems that the overall density of acidic sites of metal phosphates increases with an increase of the electronegativity of the metal cation (e.g. Al > Zr > La) but their strength does not follow the same trend. In fact, the material possessing the strongest acid sites (e.g. NH_3 desorption temperature > 400 °C) is Zr/P/O and not Al/P/O. The desorption of NH_3 at such high temperature could be related to the structure of Zr/P/O: in fact, the layered hydrogen phosphate phases (e.g. α-$Zr(HPO_4)_2$*H_2O), are known for their capacity to bond NH_3 more strongly in their interlayers than on their surface [20]. The DRIFTS spectra of pyridine desorption at increasing temperature available in the literature for Al/P/O [21], Zr/P/O [22] and La/P/O [23] show that after thermal pre-treatment these materials mostly bind pyridine with their Lewis acidic sites and that Brønsted sites, even if present, are a minority. The amount of Brønsted sites increase in the order Al > Zr > La.

To sum up, the TPD characterization of metal oxides and phosphates, in agreement with the literature, showed that the total density of acidic sites follows the order Al/P/O > Zr/P/O > La/P/O > Al_2O_3 > ZrO_2 > SiO_2 > La_2O_3, while the total density of basic sites follow the order La_2O_3 > ZrO_2 > Al_2O_3 > SiO_2 ≈ Al/P/O ≈ Zr/P/O ≈ La/P/O. In respect to metal oxides, the presence of phosphorus in metal phosphates reduced the basicity to zero regardless of the cation; on the other hand, both the density and the strength of acidic sites increased greatly. The DRIFTS characterization of adsorbed pyridine carried out on m-ZrO_2 and the literature cited suggest that all catalyst reported in this study possess mainly Lewis acidity with the exception of SiO_2 and La_2O_3 (the former is a very weak Bronsted acid, while the latter possesses negligible acidity).

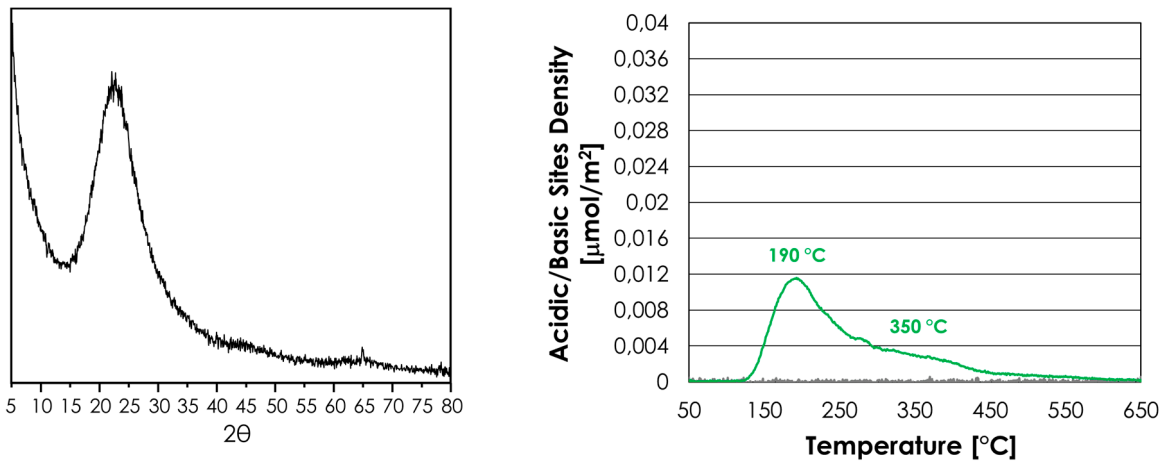

(**a**) (**b**)

Figure S2. (**a**) X-ray powder diffraction pattern of SiO_2; (**b**) CO_2 (grey line) and NH_3 (green line) temperature programmed desorption profiles for SiO_2. N.B. the highest value on the y-axis (0.04 µmol/m^2) in this case is 1/10 of the one in the graph of all the other metal oxides (0.04 µmol/m^2).

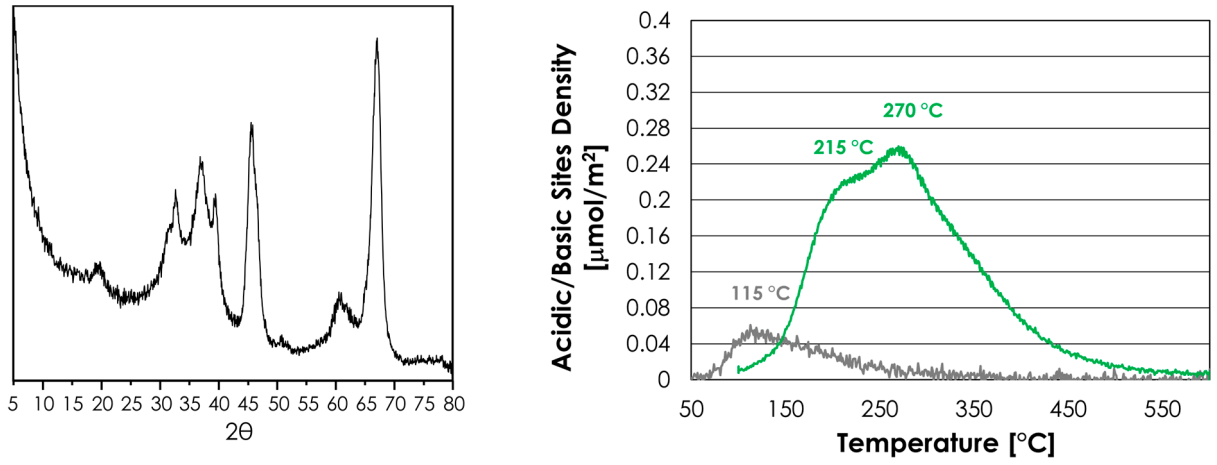

(**a**) (**b**)

Figure S3. (**a**) X-ray powder diffraction pattern of Al_2O_3; (**b**) CO_2 (grey line) and NH_3 (green line) temperature programmed desorption profiles for Al_2O_3.

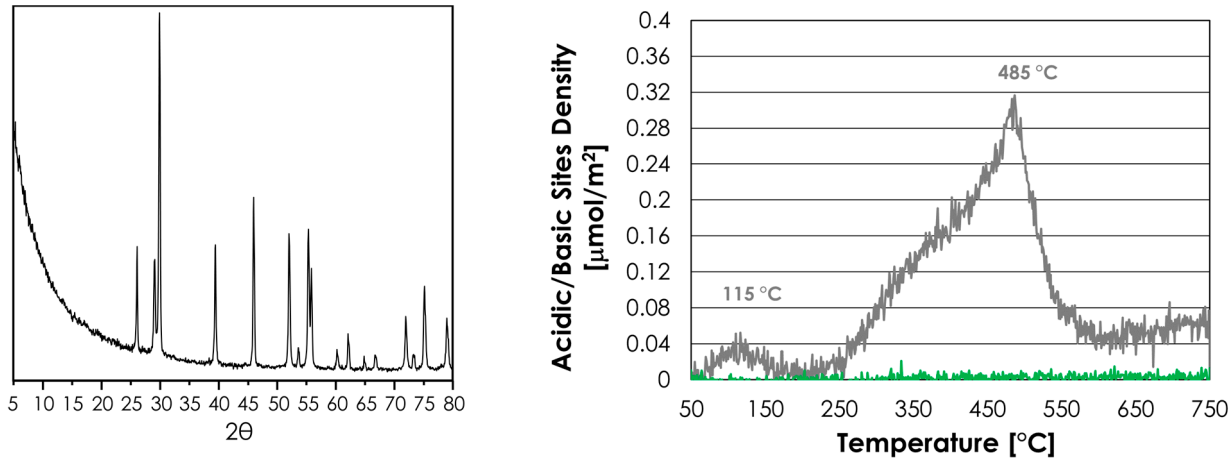

(**a**) (**b**)

Figure S4. (**a**) X-ray powder diffraction pattern of La_2O_3; (**b**) CO_2 (grey line) and NH_3 (green line) temperature programmed desorption profiles for La_2O_3.

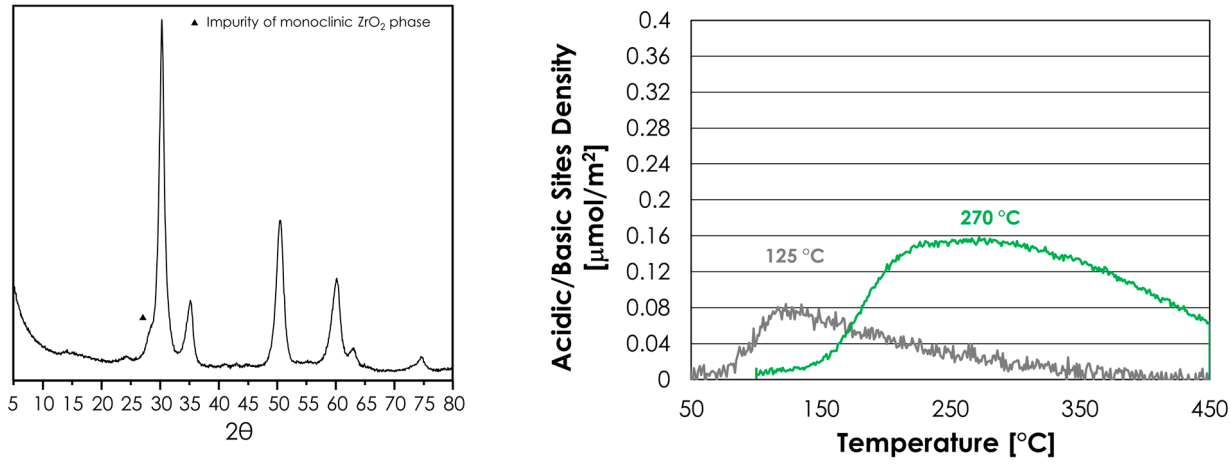

(**a**) (**b**)

Figure S5. (**a**) X-ray powder diffraction pattern of t-ZrO_2-PR; (**b**) CO_2 (grey line) and NH_3 (green line) temperature programmed desorption profiles for t-ZrO_2-PR.

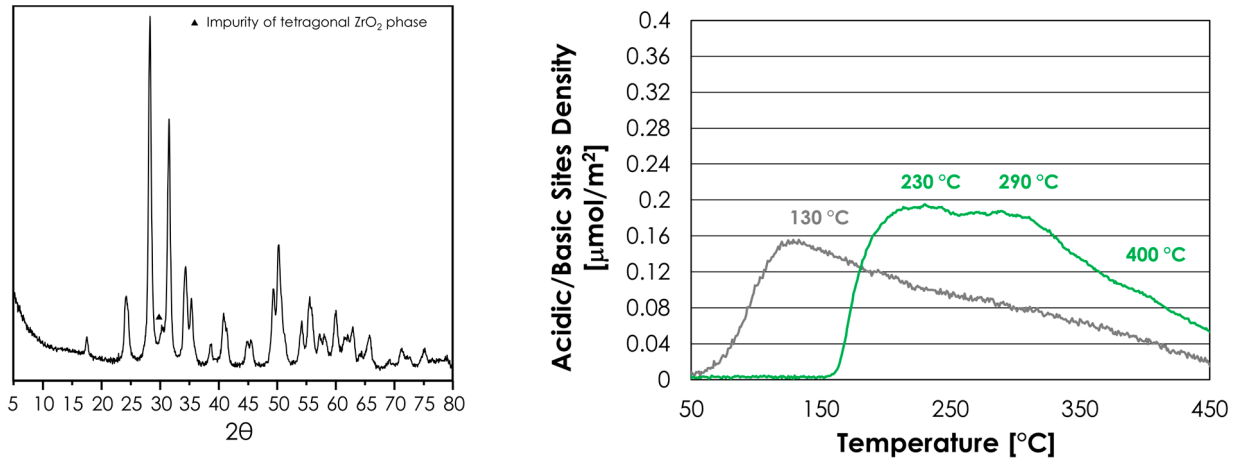

(**a**) (**b**)

Figure S6. (**a**) X-ray powder diffraction pattern of m-ZrO_2-PR; (**b**) CO_2 (grey line) and NH_3 (green line) temperature programmed desorption profiles for m-ZrO_2-PR.

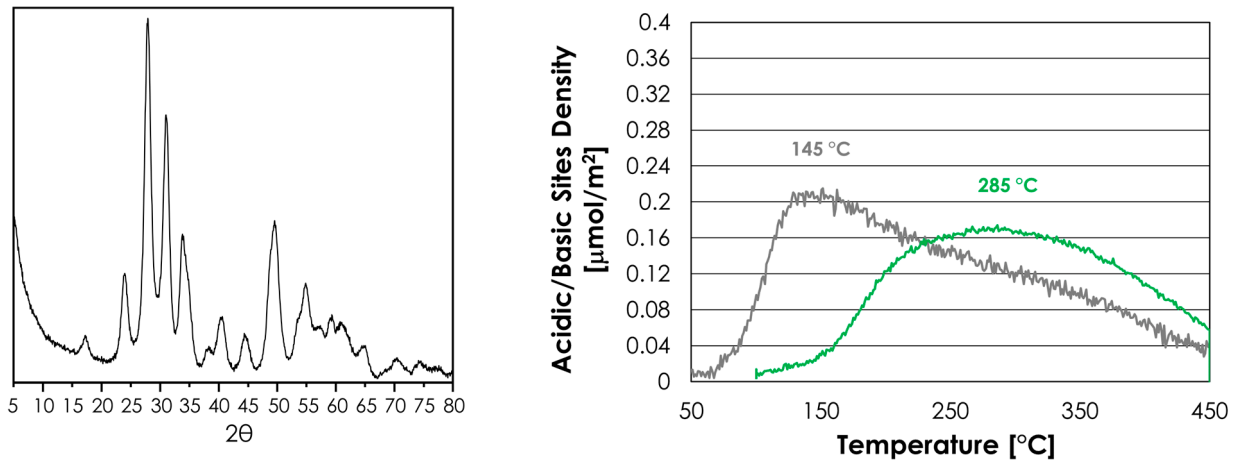

(**a**) (**b**)

Figure S7. (**a**) X-ray powder diffraction pattern of m-ZrO_2-HT; (**b**) CO_2 (grey line) and NH_3 (green line) temperature programmed desorption profiles for m-ZrO_2-HT.

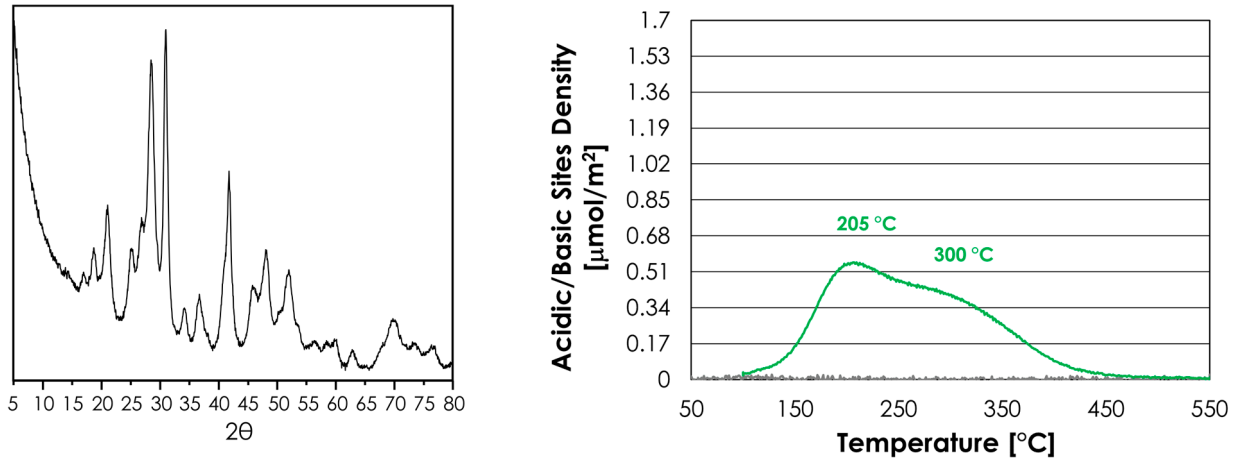

(**a**) (**b**)

Figure S8. (**a**) X-ray powder diffraction pattern of La/P/O; (**b**) CO_2 (grey line) and NH_3 (green line) temperature programmed desorption profiles for La/P/O.

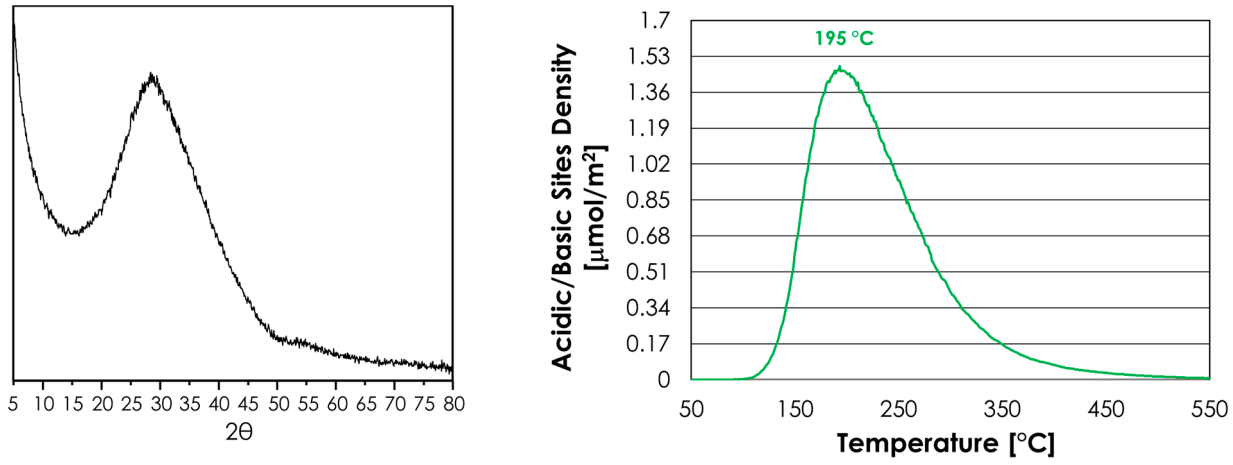

(**a**) (**b**)

Figure S9. (**a**) X-ray powder diffraction pattern of Al/P/O; (**b**) CO_2 (grey line) and NH_3 (green line) temperature programmed desorption profiles for Al/P/O.

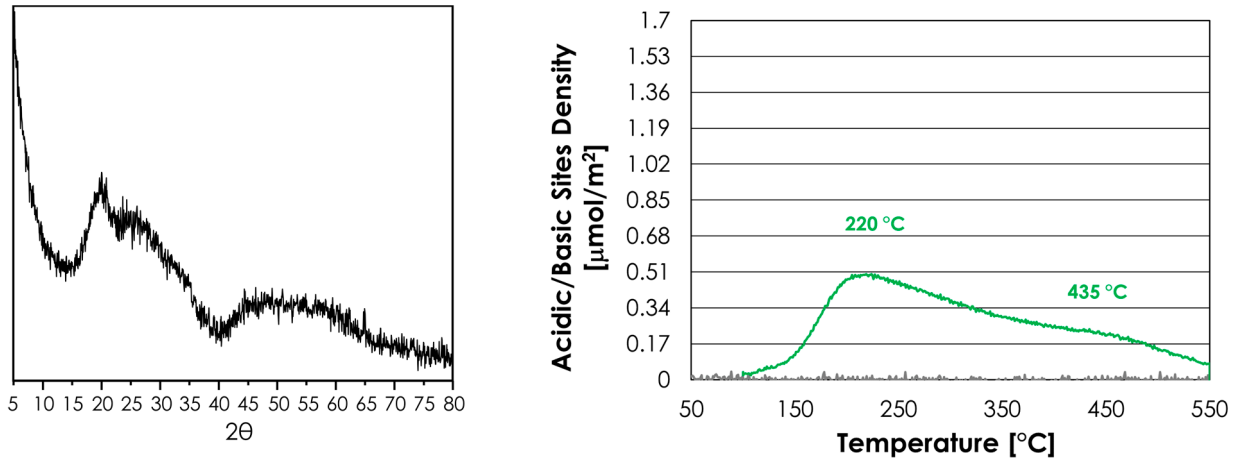

(**a**) (**b**)

Figure S10. (**a**) X-ray powder diffraction pattern of Zr/P/O; (**b**) CO_2 (grey line) and NH_3 (green line) temperature programmed desorption profiles for Zr/P/O.

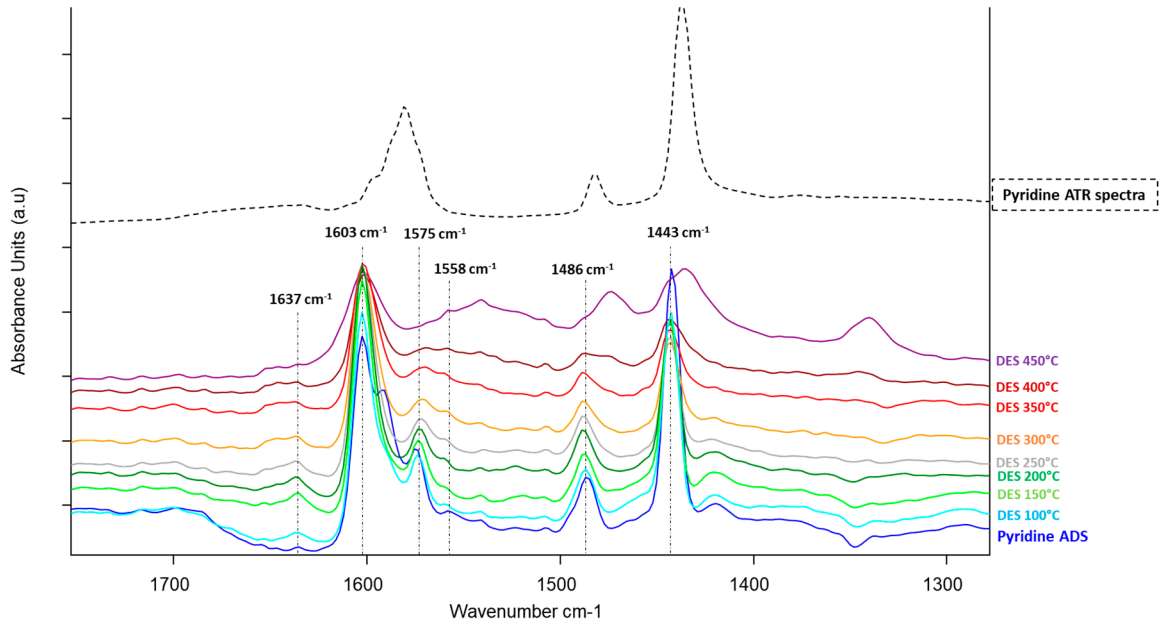

Figure S11. DRIFTS spectra recorded at increasing temperature after pyridine adsorption over m-ZrO2-HT at 50 °C. The bands attributable to pyridine bonded to Lewis acidic sites are centred at 1603 cm^{-1}, 1575 cm^{-1} and 1443 cm^{-1}. The bands attributable to Pyridine bonded to Brønsted acidic sites are centred at 1637 cm^{-1} and 1558 cm^{-1}.

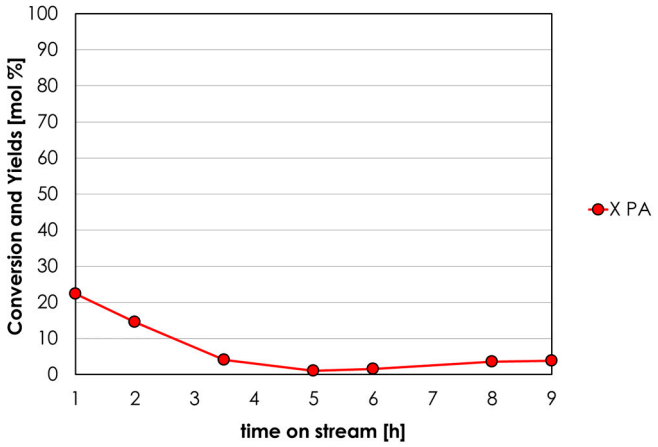

Figure S12. Blank run as a function of time on stream. Reaction conditions: temperature = 300 °C, PA = 6 mol % in N_2, time factor = W/F = 0.8 s*g/mL (calculated hypotizing to charge 1.65 g of catalyst pellets). Symbols: Propionic acid conversion (X PA, red).

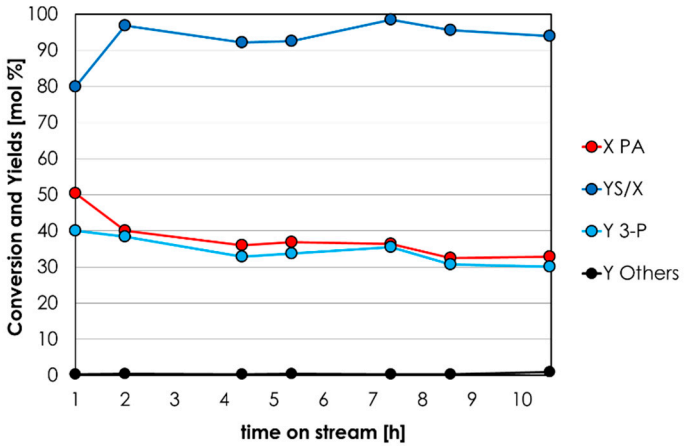

Figure S13. Catalytic activity of *m*-ZrO_2-HT for the ketonization of PA to 3-P as a function of the time on stream. Reaction conditions: temperature = 350 °C, PA = 30 mol % in N_2, time factor = W/F = 0.1 s*g/mL. Symbols: Propionic acid conversion (X PA, red), Molar Balance (YS/X, blue), 3-pentanone yield (Y 3-P, light blue); by-products sum of yields (Y Others, black).

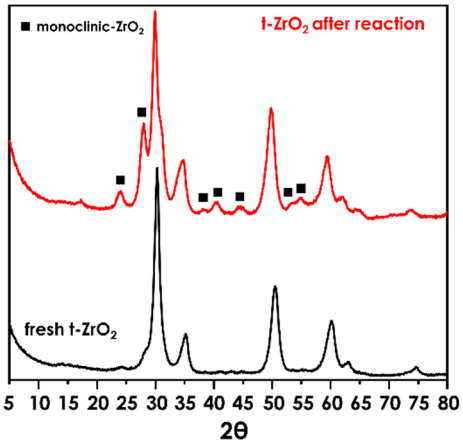

Figure S14. Powder XRD pattern of *t*-ZrO_2-PR before (black line) and after reaction (red line). Black squares indicate reflections attributable to a segregated monoclinic phase.

References

[1] V. Sushkevich, V. Ordomsky and . I. Ivanova, "Synthesis of isoprene from formaldehyde and isobutene over phosphate catalysts," *Appl. Catal. A: Gen.*, Vols. 441-442, pp. 21-29, 2012.

[2] G. Innocenti, E. Papadopoulos, G. Fornasari, F. Cavani, A. Mefford and C. Sievers, "Continuous liquid-phase upgrading of dihydroxyacetone to lactic acid over metal phosphate catalysts," *ACS Catal.*, vol. 10, pp. 11936-11950, 202.

[3] G. Parshetti, M. Suryadharma, T. Pham, R. Mahmood and R. Balasubramanian, "Heterogeneous catalyst-assisted thermochemical conversion of food waste biomass into 5-hydroxymethylfurfural," *Bioresour. Technol.*, vol. 178, pp. 19-27, 2015.

[4] J. Velasquez Ochoa, C. Bandinelli, O. Vozniuk, A. Chieregato, A. Malmusi, C. Recchi and F. Cavani, "An analysis of the chemical, physical and reactivity features of MgO–SiO2 catalysts for butadienesynthesis with the Lebedev process," *Green Chem.*, vol. 18, pp. 1653-1663, 2016.

[5] A. Tsyganenko, E. Storozheva, O. Manoilova, T. Lesage, M. Daturi and J. Lavalley, "Brønsted acidity of silica silanol groups induced by adsorption of acids," *Catal. Lett.*, vol. 70, pp. 159-163, 2000.

[6] V. Kumar, G. Naresh, M. Sudhakar, C. Anjaneyulu, S. Bhargava, J. Tardio, V. Reddy, A. Padmasri and A. Venugopal, "An investigation on the influence of support type for Ni catalysed vapour phase hydrogenation of aqueous levulinic acid to g-valerolactone," *RSC Adv.*, vol. 6, pp. 9872-9879, 2016.

[7] S. Yamaguchi, M. Yabushita, M. Kim, J. Hirajama, K. Motokura, A. Fukuoka and K. Nakajima, "Catalytic conversion of biomass-derived carbohydrates to methyl lactate by acid-base bifunctional γ-Al2O3," *ACS Sustain. Chem. Eng.*, vol. 6, pp. 8113-8117, 2018.

[8] J. Di Cosimo, G. Torres and C. Apesteguia, "One-step MIBK synthesis: A new process from 2-propanol," *J. Catal.*, vol. 208, pp. 114-123, 2002.

[9] V. Santacroce, F. Bigi, A. Casnati, R. Maggi, L. Storaro, E. Moretti, L. Vaccaro and G. Maestri, "Selective monomethyl esterification of linear dicarboxylic acids with bifunctional alumina catalysts," *Green Chem.*, vol. 18, pp. 5764-5768, 2016.

[10] Q. Mu and Y. Wang, "Synthesis, characterization, shape-preserved transformation, and optical properties of La(OH)3, La2O2CO3, and La2O3 nanorods," *J. Alloys Compd.*, vol. 509, pp. 396-401, 2011.

[11] J. Zhang and D. He, "Surface properties of Cu/La2O3 and its catalytic performance in the synthesis of glycerol carbonate and monoacetin from glycerol and carbon dioxide," *J. Colloid Interface Sci.*, vol. 419, pp. 31-38, 2014.

[12] C. Costa, T. Anastasiadou and A. Efstathiou, "The selective catalytic reduction of nitric oxide with methane over La2O3–CaO systems: synergistic effects and surface reactivity Studies of NO, CH4, O2, and CO2 by transient techniques," *J. Catal.*, vol. 194, pp. 250-265, 2000.

[13] Q. Li, N. Zhao, W. Wei and Y. Sun, "Catalytic performance of metal oxides for the synthesis of propylene carbonate from urea and 1,2-propanediol," *J. Mol. Catal. A: Chem.*, vol. 270, pp. 44-49, 2007.

[14] K. Pokrovski, K. Jung and A. Bell, "Investigation of CO and CO2 adsorption on tetragonal and monoclinic zirconia," *Langmuir*, vol. 17, pp. 4297-4303, 2001.

[15] B. Bachiller-Baeza, I. Rodriguez-Ramos and A. Guerrero-Ruiz, "interaction of carbon dioxide with the surface of zirconia polymorphs," *Langmuir*, vol. 14, pp. 3556-3564, 1998.

[16] S. Ding, H. Wang, J. Han, X. Zhu and Q. Ge, "Ketonization of propionic acid to 3-pentanone over CexZr1−xO2 Catalysts: the importance of acid-base balance," *Ind. Eng. Chem. Res.*, vol. 57, pp. 17086-17096, 2018.

[17] P. Blair Vasquez, T. Tabanelli, E. Monti, S. Albonetti, D. Bonincontro, N. Dimitratos and F. Cavani, "Gas-phase catalytic transfer hydrogenation of methyl levulinate with ethanol over ZrO2," *ACS Sustain. Chem. Eng.*, vol. 7, pp. 8317-8330, 2019.

[18] S. Ding, J. Zhao and Q. Yu, "Effect of the zirconia polymorph on vapor-phase ketonization of propionic acid," *Catalysts*, vol. 9, p. 768, 2019.

[19] G. Busca, "The surface acidity of solid oxides and its characterization by IR spectroscopic methods. An attempt at systematization," *Phys. Chem. Chem. Phys.*, vol. 1, pp. 723-736ù, 1999.

[20] M. Turco, P. Ciambelli, G. Bagnasco, A. La Ginestra, P. Galli and C. Ferragina, "TPD study of NH3 adsorbed by different phases of zirconium phosphate," *J. Catal.*, vol. 117, pp. 355-361, 1989.

[21] R. Estevez, S. Lopez-Pedrajas, F. Blanco-Bonilla, D. Luna and F. Bautista, "Production of acrolein from glycerol in liquid phase on heterogeneous catalysts," *Chem. Eng. J.*, vol. 282, pp. 179-186, 2015.

[22] C. Antonetti, M. Melloni, D. Licursi, S. Fulignati, E. Ribechini, S. Rivas, J. Parajo, F. Cavani and A. Raspolli Galletti, "Microwave-assisted dehydration of fructose and inulin to HMFcatalyzed by niobium and zirconium phosphate catalysts," *Appl. Cat. B,* vol. 206, pp. 364-377, 2017.

[23] Z. Guo, D. Theng, K. Tang, L. Zhang, L. Huang, A. Borgna and C. Wuang, "Dehydration of lactic acid to acrylic acid over lanthanum phosphate catalysts: the role of Lewis acid sites," *Phys. Chem. Chem. Phys.,* vol. 18, p. 23746, 2016.